Article

Iridium Catalysts for C–C and C–O Hydrogenolysis: Catalytic Consequences of Iridium Sites

Aracelis J. Pamphile-Adrián, Pedro P. Florez-Rodriguez and Fabio B. Passos*

*Departamento de Engenharia Química e de Petróleo, Universidade Federal Fluminense,
Rua Passos da Pátria, 156, 24210-040 Niterói-RJ, Brazil*

The support effect on the properties of iridium catalysts for C–C and C–O hydrogenolysis was investigated. Cyclohexane conversion and glycerol hydrogenolysis were used to compare the behavior of iridium catalysts in terms of C–C and C–O cleavage. The nature of the support influenced the catalyst performance in both cyclohexane conversion and glycerol hydrogenolysis. This effect was more evident on the product selectivity. Ir/SiO_2 catalyst presented the highest cyclohexane hydrogenolysis activity and the highest selectivity to minor hydrocarbons formed from hexane re-adsorption. For glycerol hydrogenolysis, all catalysts displayed a higher selectivity to products formed by C–O cleavage, mainly 1,2-propanediol (1,2-PDO). Ir/ZrO_2 catalyst presented the highest activity in all reaction conditions and the lowest selectivity to minor alcohols produced by C–C cleavage like methanol, ethanol and ethylene glycol. The results were explained in terms of the requirements and the structure of the catalytic sites.

Keywords: iridium catalysts, hydrogenolysis, C–C cleavage, C–O cleavage, support effect

Introduction

Iridium catalysts have been tested for several reactions like isomerization,[1,2] hydrogenation,[3-6] hydrazine decomposition and several authors reported their high activity for hydrocarbon hydrogenolysis reactions.[7-12] For example, McVicker *et al.*[12] studied the selective rupture of naphthenic rings (methylcyclopentane (MCP), methylcyclohexane (MCH), 1,1-, 1,2- and 1,3-dimethylcyclopentane (1,1-DMCP, 1,2-DMCP and 1,3-DMCP), pentylcyclopentane (PCP) and ethylcyclopentane (ECP)) on Pt/SiO_2, Pt/Al_2O_3, Ni/Al_2O_3, Ru/Al_2O_3, Rh/Al_2O_3 and Ir/Al_2O_3. Among the mentioned catalysts, Ir/Al_2O_3 presented the best activity and selectivity for cleavage of non-substituted C–C in five-membered naphthenic rings as MCH and PCP.[12]

Cyclohexane, a model six-membered naphthenic molecule, has been used to study the direct endocyclic C–C bond cleavage.[13,14] Additionally, conversion of cyclohexane is typically used to probe the catalyst surface properties such as apparent dispersion (dehydrogenation to benzene) and surface structure (hydrogenolysis).[15–20]

Several studies of cyclohexane conversion on Ir catalysts were performed to understand the dependence of cyclohexane hydrogenolysis activity and reaction mechanism on factors like dispersion, particle size and H_2/cyclohexane ratio.[13,14,21] Locatelli *et al.*[21] investigated cyclohexane hydrogenolysis over Ir/SiO_2 and proposed a reaction mechanism in which the key step is a concerted electronic transfer in a dimetallacyclopentane intermediate. Thus, after hexane formation subsequent hydrogenolysis steps define the minor hydrocarbons that are formed.

On the other hand, less attention have been paid to fundamental investigation of C–O hydrogenolysis over Ir catalysts. Ir-ReO_x/SiO_2 are active in C–O hydrogenolysis of substrates like glycerol, tetrahydrofurfuryl alcohol, tetrahydrofuran and tetrahydropyran.[22-26] Among these substrates, glycerol is a versatile feedstock that is mainly obtained as a by-product of biodiesel production. Consequently, due to the fast growth of biodiesel production worldwide, catalytic transformation of glycerol into high-value products has gained importance in the last decade.

Glycerol hydrogenolysis may yield 1,2- and 1,3-propanediol (1,2-PDO and 1,3-PDO), high-value raw materials for the chemical industry.[27] The formation of these and other alcohols requires one or more C–O cleavages, and particularly, 1,3-PDO is difficult to obtain due to the difficult cleavage of the secondary C–O bond.

Nakagawa *et al.*[22] studied the 1,3-PDO production over Ir-ReO_x/SiO_2 and found the addition of several acids

*e-mail: fbpassos@vm.uff.br

as H_2SO_4, silica-alumina, zeolites and ion-exchange resin promoted the activity of the catalyst.[24] According to these authors, the mechanism of glycerol hydrogenolysis to 1,3-propanediol occurs through attack of hydride species at the interface between Ir metal surface and ReO_x to the adsorbed glycerol on the ReO_x cluster.[23]

In this work, we report cyclohexane conversion and glycerol hydrogenolysis over iridium catalysts supported on γ-Al_2O_3, SiO_2 and ZrO_2, comparing these catalysts in terms of C–C and C–O cleavage. We also address the effect of support on the activity and product selectivity in both reactions. This study contributes to a better understanding of the catalytic consequences for both reactions of modification of Ir catalytic sites.

Experimental

Catalyst preparation

Commercial γ-Al_2O_3 (Puralox HP-14) and SiO_2 (DAVICAT), used as catalyst supports, were calcined at 600 and 900 °C, respectively, during 4 h (5 °C min⁻¹). ZrO_2 was synthesized by precipitation of $Zr(OH)_4$. NH_4OH (25% v/v) was added to an aqueous solution of $ZrO(NO_3)_2 \cdot xH_2O$ until a pH equal to 14 was reached. The precipitated solid was filtered, washed with deionized water and dried overnight at 100 °C. The prepared $Zr(OH)_4$ was calcined at 500 °C during 4 h (5 °C min⁻¹). The calcination temperatures were chosen to obtain similar surface areas of the supports. The catalysts were prepared by incipient wetness impregnation technique using a solution of $H_2IrCl_6 \cdot xH_2O$ (Sigma-Aldrich) to yield 2 wt.% Ir. The impregnated solids were dried at 70 °C for 16 h due to the low melting point of $H_2IrCl_6 \cdot xH_2O$ (65 °C). Finally, the catalysts were calcined at 400 °C during 4 h (5 °C min⁻¹).

Catalyst characterization

Nitrogen adsorption isotherms of the samples were measured using a Micromeritics ASAP 2020 equipment. Surface areas were calculated using the Brunauer-Emmett-Teller (BET) equation. X-Ray diffraction (XRD) experiments were performed using a Miniflex RIGAKU spectrometer (Cu Kα radiation). The diffractograms were obtained between 2θ = 10 and 80° using a 0.04° step size (1 s *per* step).

Temperature programmed reduction (TPR), H_2 pulse chemisorption and temperature programmed desorption (H_2-TPD) experiments were performed with a multipurpose unit coupled to a Prisma quadrupole mass spectrometer (Pfeiffer). For TPR analysis, the samples were dried at

150 °C for 30 min under He flow (30 mL min⁻¹) and cooled to room temperature. Then, the samples were submitted to a 5% H_2/Ar gas flow (30 mL min⁻¹) and the temperature was raised to 1000 °C at a heating rate of 10 °C min⁻¹. For H_2-TPD experiments, the samples were dried as mentioned before and were reduced at 250 °C. After reduction, a He stream (30 mL min⁻¹) was passed through the catalyst during 30 min at the reduction temperature and then cooled to 27 °C. H_2 pulses from a 100 μL loop were injected in a He stream (30 mL min⁻¹) until the area of the pulses remained constant, indicating saturation of the catalyst surface. Then, the temperature was increased to 1000 °C at a heating rate of 10 °C min⁻¹, under He flow, while H_2 desorption was monitored.

X-Ray photoelectron spectroscopy (XPS) analysis was carried out using an ESCALAB 250Xi spectrometer (Thermo Fisher Scientific) with monochromatic Al Kα X-rays (spot size of 900 μm). Surface charging of the electrically insulating materials was compensated using the integrated flood gun with approximate spot size of 900 μm. Survey spectra were obtained with a pass energy of 100 eV and region spectra (Ir4f, Al2p, Si2p, Zr3d) using a pass energy of 58 eV. The base pressure of the analysis chamber was 7×10^{-10} mbar. Spectra were acquired, analyzed and peak fitted using the Avantage software with Lorentzian/Gaussian product function and a Shirley type background. Ir4f spectra were fitted with an energy constraint for Ir4f$_{5/2}$ within a 3 eV shift relative to the Ir4f$_{7/2}$ peak, an area ratio of 0.75:1, respectively, and a full width at half maximum (FWHM) in the range 0.5-2.5 eV. The residual standard deviation of the fitted Ir4f spectra was around 0.9 for all catalysts.

Fresh and used catalysts were characterized by Raman spectroscopy with a WITec alpha 300 system. Experiments were performed at 25 °C using 50× objective lens (numerical aperture = 0.75) and a Nd:YAG green laser with 532 nm wavelength with an aperture of 800 cts to avoid the decomposition of possible organic compounds in the sample. The integration time was 0.777 s and the number of scans was 600.

Cyclohexane conversion

This reaction was performed under atmospheric pressure in a continuous flow microreactor. The pre-treatment of the samples (10 mg) consisted of drying at 150 °C under 30 mL min⁻¹ of He flow for 30 min, followed by reduction at 250 °C under H_2 flow (30 mL min⁻¹). The reactant mixture was obtained by bubbling hydrogen through a saturator containing cyclohexane at 11 °C (H_2/C_6H_{12} = 14.2). The total flow rate was 100 mL min⁻¹. At these conditions, the conversion was kept below 10%.

The reaction system was gradually heated and samples were collected at 250, 260, 270, 280, 290, 300 and 310 °C. A descending temperature sequence was also performed to detect any deactivation. The reaction products were analysed in a gas chromatograph (GC) HP GC-5890 Series II, equipped with an HP-Innowax capillary column and a flame ionization detector. The products were also analysed in a Micro-GC 490 (Agilent), equipped with three columns: M5A for permanent gases (H_2, O_2, N_2, CH_4 and CO), 5CB for hydrocarbons (C_3-C_6) and PPU for CO_2 and ethane.

The conversion was kept below 10%, which enabled comparison of the selectivities at similar conversions.[16] The selectivity for the hydrogenolysis products was calculated as the ratio between the amount of cyclohexane converted to a hydrogenolysis product and the total amount of reacted cyclohexane, according to the equation below:

$$Selectivity\ (\%) = \frac{j_i \times F_i}{6F_{A_0} \times X_{A_{Hydrogenolysis}}} \times 100 \tag{1}$$

in which j_i is the number of carbons in product i, F_i is the exit flow rate of product i, F_{A_0} is the initial flow rate of cyclohexane and $X_{A_{Hydrogenolysis}}$ is the cyclohexane conversion to hydrogenolysis products.

Glycerol hydrogenolysis

Glycerol hydrogenolysis reactions were performed in a 300 mL autoclave reactor (Parr Instruments Co.). The catalyst was reduced in the autoclave prior the reaction. The reactor was loaded with the necessary amount of water and catalyst, and then was filled with H_2, with 200 psi of pressure, the stirring speed was adjusted to 500 rpm and the temperature was set to 250 °C. After 2 h, the reactor was cooled to 25 °C, opened, and glycerol was quickly loaded into the reactor. Then, the reactor was filled with the desired pressure of H_2, both the stirring speed and pressure were adjusted, and the temperature was set to the desired value. After the reaction time (12 h), the reactor was cooled to room temperature, gas phase was collected and analyzed in the Micro-GC 490. The liquid phase products were quantified in a gas chromatograph-mass spectrometer (GC-MS) QP2010Plus (Shimadzu) equipped with a capillary column (Rtx-Wax). The products were identified using GC-MS Solutions software comparing with the National Institute of Standards and Technology NIST05 and NIST05s libraries. Initial turnover frequency (TOF) values were estimated for each catalyst from the initial reaction rate, assuming a first order reaction, and using H_2 chemisorption to estimate the number of surface iridium sites. Product selectivity was calculated on carbon basis using the following equation:

$$Selectivity\ (\%) = \frac{j_i \times y_i}{\sum_i j_i \times y_i} \times 100 \tag{2}$$

in which j_i is the number of carbons of product i and y_i is the molar fraction of product i.

For all reactions, gas phase products (CO, CO_2 and CH_4) were not considered for calculations, since their selectivities were negligible (< 0.5%).

Results and Discussion

Characterization of catalysts

X-Ray diffractograms of the catalysts (not shown) displayed the respective main peaks of the supports: SiO_2, γ-Al_2O_3 and ZrO_2 (tetragonal and monoclinic phases). However, characteristic peaks of iridium species were not observed due to the low iridium content or to a high dispersion of iridium species on the support.[28,29]

XPS spectra for Ir4f of the calcined catalysts are presented in Figure 1. In the case of the Ir/γ-Al_2O_3 (Figure 1b), the Ir4f doublet was not resolved, showing a first evidence of the effect of the support on the characteristics of the surface of the catalysts. The presence of two different iridium species on the surface of the catalyst was evidenced by the deconvolution of the Ir4f peaks. The two doublets (including $Ir4f_{5/2}$ and $Ir4f_{7/2}$) were identified in Figure 1 as A and B. The doublets identified as A, of lower energy, can be attributed to surface IrO_2.[30-32] The doublets identified as B in all spectra can be attributed to the presence of surface iridium chloride species ($IrCl_3$ or $IrCl_4$), as reported by Folkesson[33] and Kim and Hatfield.[34] The presence of these chloride species was observed in the survey spectrum of all catalysts, with spectral lines of Cl2p (200 eV) and Cl2s (270 eV), indicating that after calcination the chloride species remain on the surface of the catalyst. In the case of Ir/ZrO_2, the spectrum showed a higher amount of $IrCl_4$ than IrO_2, 87 and 13%, respectively (Table 1), which confirms that the calcination of the catalyst was not efficient to completely eliminate the metal precursor.

Surface and bulk Ir/Si, Ir/Al and Ir/Zr atomic ratios are shown in Table 1. The surface to bulk ratio increased in the order Ir/Zr < Ir/Al < Ir/Si, the same order obtained by H_2 pulse chemisorption.

TPR profiles (Figure 2a) of the catalysts showed an increment in the reduction temperature peaks in the sequence Ir/ZrO_2 < Ir/SiO_2 < Ir/γ-Al_2O_3 (100, 195 and 254 °C, respectively), which can indicate an increase in

Table 1. XPS results for prepared catalysts

Catalyst	Ir/M[a]			Ir4f$_{7/2}$ (IrO$_2$) BE / eV	At.%[b]	Ir4f$_{7/2}$ (IrCl$_x$) BE / eV	At.%[b]
	Bulk	Surface	$\frac{Surface}{Bulk} \times 100$ / %				
Ir/SiO$_2$	0.008	0.0056	69.3	61.6	72	63.7	28
Ir/γ-Al$_2$O$_3$	0.004	0.0026	65.3	61.3	60	63.1	40
Ir/ZrO$_2$	0.013	0.0077	58.8	60.3	13	62.1	87

[a]Calculated from atomic percentages obtained in survey spectra using Ir4f, Si2p, Al2p and Zr3p peaks; M = Si, Al, Zr; [b]calculated atomic percentages using respective Ir4f$_{7/2}$ peaks. BE: binding energy.
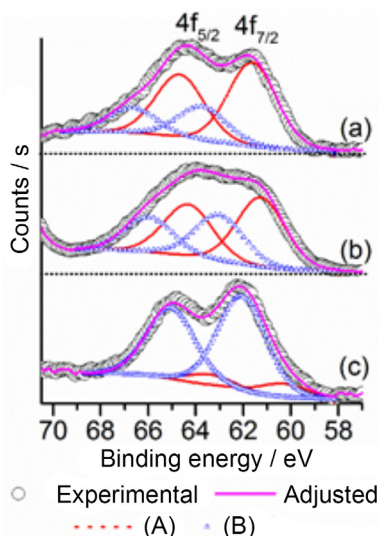

Figure 1. XPS spectra of the Ir4f spectral line of iridium catalysts: (a) Ir/SiO$_2$; (b) Ir/γ-Al$_2$O$_3$; (c) Ir/ZrO$_2$. The doublets can be attributed to (A) surface IrO$_2$ or (B) surface IrCl$_3$ or IrCl$_4$.

the interaction of the metal precursor and the support.[35] In all cases, the reduction peaks can be attributed to the reduction of iridium oxide and iridium chloride species with different interactions with the support,[4] whose presence was also confirmed by the XPS experiments. In the case of Ir/γ-Al$_2$O$_3$ (Figure 2a), the reduction peak was broader than the reduction peaks of the other two catalysts. The surface areas obtained for all catalysts were within the desired range for this investigation: Ir/ZrO$_2$ (81 m^2 g^{-1}), Ir/SiO$_2$ (167 m^2 g^{-1}) and Ir/γ-Al$_2$O$_3$ (119 m^2 g^{-1}).

Hydrogen chemisorption results are summarized in Table 2. In general, metal dispersion followed the same trend as surface area of the supports, since higher surface areas often lead to higher metal dispersion.[36,37] Ir/SiO$_2$ presented the highest surface area and dispersion among the studied catalysts, but the values were similar to those obtained for Ir/γ-Al$_2$O$_3$. H$_2$ chemisorption uptakes were used to estimate iridium average particle diameters (Table 2), resulting in similar sizes for Ir/γ-Al$_2$O$_3$ and Ir/SiO$_2$ and somewhat larger size for Ir/ZrO$_2$. H$_2$-TPD profiles for the catalysts are presented in Figure 2b. The
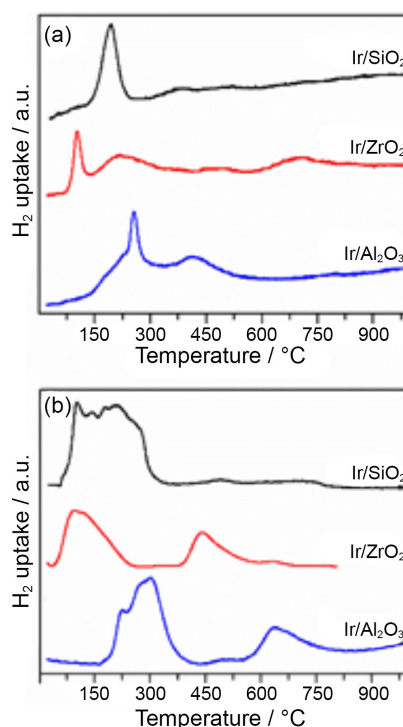

Figure 2. (a) H$_2$-TPR and (b) H$_2$-TPD profiles of iridium catalysts.

TPD profile of Ir/SiO$_2$ showed a broad peak between 50 and 360 °C due to desorption of H$_2$ from different types of active sites present on the catalyst surface, indicating the surface is non-uniform. In the case of Ir/ZrO$_2$, the TPD profile showed two main desorption peaks. The first one, placed at around 100 °C, can be attributed to desorption of H$_2$ from the metal surface, and the second peak can be due to desorption of spillover hydrogen from the support. Finally, the TPD profile of Ir/γ-Al$_2$O$_3$, Figure 2b, showed a main peak around 304 °C, with a shoulder at 220 °C. The peak can be attributed to strongly adsorbed hydrogen on metallic iridium, and the shoulder can be due to weakly adsorbed hydrogen. This profile also presented a peak around 630 °C that is attributed to desorption of spillover hydrogen from the support.[38] Comparing the TPD profiles of all catalysts, H$_2$ desorption temperature increased in the sequence Ir/ZrO$_2$ < Ir/SiO$_2$ < Ir/γ-Al$_2$O$_3$, which can

Table 2. Surface characterization of fresh Ir supported catalysts by H_2 pulse chemisorption and cyclohexane conversion

Catalyst	H_2 uptake / (μmol $g_{catalyst}^{-1}$)	(H/Ir) × 100 / %	d_p^a / nm	Cyclohexane rate of reaction^b / (mmol h^{-1} g$_{cat}^{-1}$)		TOF^c / s^{-1}		Ea / (kcal mol^{-1})	
				Dehyd.	Hydr.	Dehyd.	Hydr.	Dehyd.	Hydr.
Ir/γ-Al$_2$O$_3$	35	67	1.5	29.3	2.9	0.12	0.012	20	17
Ir/SiO$_2$	37	71	1.4	22.6	4.4	0.09	0.018	17	11
Ir/ZrO$_2$	30	57	1.8	44.0	2.8	0.18	0.011	21	15

^{a}Particle size calculated as $d_p = 1 / (H / Ir)$; ^{b}calculated at 260 °C; ^{c}turnover frequency calculated from H_2 chemisorption. Ea: activation energy; Dehyd.: cyclohexane dehydrogenation; Hydr.: cyclohexane hydrogenolysis.

indicate different binding strength between hydrogen and the metal sites.

Cyclohexane conversion

Cyclohexane conversion results are summarized in Table 2. Although the dehydrogenation reaction rate is often used as an indicator of metal dispersion, the highest dehydrogenation rate was obtained with Ir/ZrO$_2$. This catalyst presented the lowest dispersion as measured by H_2 chemisorption. This was probably caused by the Ir–Zr$^+$ interactions, which could provide the formation of new interfacial sites, which are active for dehydrogenation but inactive for hydrogen adsorption.[39]

The results for cyclohexane hydrogenolysis rate showed a different trend. The higher hydrogenolysis rate and the lower activation energy obtained for Ir/SiO$_2$ are consistent with the increase of TOF with the dispersion observed for small Ir particles.[14,40] The structure sensitivity for hydrogenolysis varies with metal and type of reactant. For example, Sinfelt[41] studied the hydrogenolysis of ethane reaction over a series of SiO$_2$ supported Rh catalysts with different metal concentrations (varying from bulk to 0.1 wt.% Rh). For that series of catalysts, the catalytic activity increased with the decrease of particle size for bulk Rh (256.0 nm), 5 wt.% Rh/SiO$_2$ (sintered, 12.7 nm) and 1-10 wt.% Rh/SiO$_2$ (1.2-4.1 nm) catalysts. Within the latter series, the specific activity for the ethane hydrogenolysis varied from 8 to 16 mmol of ethane converted *per* hour *per* square meter of rhodium, increasing with the decrease of particle size.

Figure 3 displays the dependence of product selectivity of cyclohexane hydrogenolysis with temperature for all catalysts. A first difference is observed between Ir/SiO$_2$ (that presented the best activity for cyclohexane hydrogenolysis) and the other catalysts regarding the formation of minor hydrocarbons from hexane fragmentation. The selectivity to methane increased with temperature, showing significant cyclohexane fragmentation for this catalyst, in agreement with the results reported by Locatelli *et al.*[21] for cyclohexane
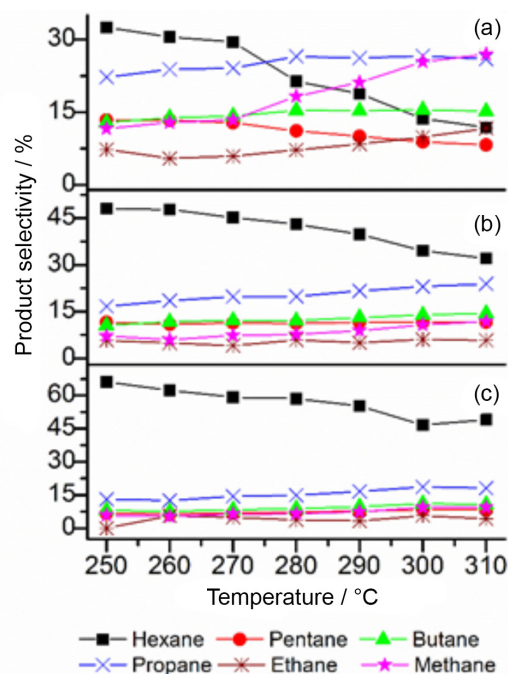

Figure 3. Product selectivity for cyclohexane hydrogenolysis at 260 °C. (a) Ir/SiO$_2$; (b) Ir/γ-Al$_2$O$_3$; (c) Ir/ZrO$_2$.

conversion over Ir/SiO$_2$. Methane and pentane selectivities did not follow complementary trends for temperatures higher than 280 °C. This indicates methane was formed via successive terminal hydrogenolysis of intermediate hexane.[21]

On the other hand, Ir/ZrO$_2$ and Ir/γ-Al$_2$O$_3$ catalysts showed a different behavior (Figures 3b and 3c). For both catalysts, hexane was the main hydrogenolysis product throughout the temperatures range, showing a lower ability of these catalysts for C–C cleavage from hexane, which is in agreement with the values of TOF and reaction rate obtained for this reaction. For these two catalysts, the fragmentation of cyclohexane occurred by C–C cleavage from hexane re-adsorption, giving similar selectivities for the methane-pentane and ethane-butane pairs. This mechanism could be explained by the formation of two different types of hexane re-adsorption on the catalyst surface, one that leads to a C_I–C_{II} cleavage (to form

pentane and methane), and another one that leads to a C_{II}–C_{III} cleavage (to form ethane and butane) or a C_{III}–C_{IV} cleavage (to form propane).[35] This way, after the primary hydrogenolysis of cyclohexane to hexane, while on Ir/SiO$_2$ catalysts methane is further formed through terminal C–C hydrogenolysis, in the case of Ir/γ-Al$_2$O$_3$ and Ir/ZrO$_2$ internal C–C cleavage was favored. This can be explained by the formation of metal-support adlineation sites on Ir/γ-Al$_2$O$_3$ and Ir/ZrO$_2$ catalysts which hinder the required intermediate for terminal C–C cleavage.

Glycerol hydrogenolysis

Table 3 lists the conversion and selectivity of glycerol hydrogenolysis over the tested catalysts. Total mass balance closed between 97 and 101% for all reactions. The activity of the catalysts was measured by the TOF based on H$_2$ chemisorption uptakes. All catalysts presented a very low activity for the hydrogenolysis of glycerol in these reaction conditions compared with Ru catalysts tested in the same conditions.[42] However, the results can be used to better understand the requirements of the iridium catalytic sites. TOF and conversion values increased in the sequence Ir/SiO$_2$ < Ir/γ-Al$_2$O$_3$ < Ir/ZrO$_2$. The trend in glycerol hydrogenolysis activity was the same as the one observed for the dehydrogenation of cyclohexane, which could indicate that there is an influence of the number of available Ir active sites on the catalysts surfaces on glycerol adsorption or products desorption. Besides, the presence of adlineation metal-support sites on Ir/γ-Al$_2$O$_3$ and Ir/ZrO$_2$ favored glycerol conversion. Raman spectroscopy analysis of spent catalysts did not evidence any presence of carbon compounds. For all catalysts, 1,2-propanediol (1,2-PDO) was the main product. Despite the low activity, Ir/SiO$_2$ showed the highest selectivity to 1,2-PDO (86.7%). Ir/γ-Al$_2$O$_3$ and Ir/ZrO$_2$ presented 1,2-PDO selectivities of 79.4 and 71.6%, respectively. These results indicate that all catalysts favored the selective primary C–O cleavage over C–C cleavage.

For all catalysts, the formation of propanol and methanol can be explained by the subsequent hydrogenolysis of 1,2-PDO and/or 1,3-PDO.[43,44] Among the three catalysts, Ir/γ-Al$_2$O$_3$ presented the greater ability for C–C cleavage, forming methanol and ethylene glycol with selectivities of 9.0 and 3.2%, respectively. This result can indicate a better carbon adsorption on the catalyst surface to allow the C–C cleavage and the consequent formation of the mentioned products, which can be related to the properties of the supports. Delgado *et al.*[45] found similar results for glycerol hydrogenolysis reaction on a series of Pt catalysts supported on TiO$_2$, Al$_2$O$_3$ and SiO$_2$-Al$_2$O$_3$. Pt/TiO$_2$, with less acidic sites than the other catalysts, presented higher selectivity to C$_3$ products, whereas the catalysts with more acidic sites yielded the formation of minor alcohols like methanol. The same argumentation could explain the behavior of our series of catalysts, in terms of the difference on the formation of the minor alcohols from subsequent hydrogenolysis of 1,2-PDO.

Ir/SiO$_2$ catalyst was used to investigate the effect of increasing the H$_2$ initial pressure from 360 to 550 psi (Table 4). Increasing H$_2$ pressure caused a decrease in glycerol conversion and in selectivity to 1,2-PDO, which decreased from 86.7 to 82%. An interesting difference between these two reactions is observed in the selectivity to acetol, a glycerol dehydration product, which was higher for the reaction performed at higher pressure. This result could indicate that higher pressures have an unfavorable effect on the subsequent hydrogenation of acetol to form 1,2-PDO. For this series of spent catalysts, no characteristic bands of carbon compounds were observed in Raman spectroscopy analysis.

The support effect on glycerol hydrogenolysis was also studied at higher temperature and pressure conditions (Table 5). The total mass balance closed between 98 and 102% for all reactions. In these conditions, glycerol conversion increased in the following sequence: Ir/SiO$_2$ < Ir/γ-Al$_2$O$_3$ < Ir/ZrO$_2$. The higher activity of Ir/ZrO$_2$ is in agreement with several studies which showed Ir/ZrO$_2$ is an active catalyst for hydrogenation reactions.[46,47] In this series of reactions, the increase on conversion and the formation of esters, carboxylic acids and long chain alcohols (C$_{4+}$) could be due to the elevated temperature of

Table 3. Effect of the support on conversion and selectivity of glycerol hydrogenolysis. Reaction conditions: T = 200 °C; PH$_2$ = 360 psi; m$_{catalyst}$ = 1 g; 150 mL of 20% glycerol solution; t$_{reaction}$ = 12 h

Catalyst	Conversion / %	TOF / s^{-1}	Product selectivity / %						
			1,2-PDO	1,3-PDO	PrOH	EG	MeOH	Acetol	Others
Ir/SiO$_2$	3.9	0.004	86.7	0.0	6.4	1.1	0.0	5.9	0.0
Ir/γ-Al$_2$O$_3$	7.7	0.009	79.4	1.1	5.1	3.2	9.0	2.1	0.0
Ir/ZrO$_2$	8.3	0.012	71.6	2.2	16.2	2.8	0.0	3.7	3.5

TOF: turnover frequency; PDO: propanediol; PrOH: propanol; EG: ethylene glycol; MeOH: methanol.

Table 4. Effect of H_2 initial pressure on conversion and selectivity of the glycerol hydrogenolysis over Ir/SiO_2 catalyst. Reaction conditions: T = 200 °C; $m_{catalyst}$ = 1 g; 150 mL of 20% glycerol solution; $t_{reaction}$ = 12 h

PH_2 / psi	Conversion / %	TOF / s^{-1}	Product selectivity / %					
			1,2-PDO	EtOH	MeOH	PrOH	EG	Acetol
360	3.9	0.004	86.7	0.0	0.0	6.4	1.1	5.9
550	1.5	0.003	82.0	0.9	0.6	7.0	0.0	9.4

TOF: turnover frequency; PDO: propanediol; EtOH: ethanol; MeOH: methanol; PrOH: propanol; EG: ethylene glycol.

Table 5. Effect of support on conversion and selectivity of glycerol hydrogenolysis. Reaction conditions: T = 250 °C; PH_2 = 550 psi; $m_{catalyst}$ = 1 g; 150 mL of 50% glycerol solution; $t_{reaction}$ = 12 h

Catalyst	Conversion / %	TOF / s^{-1}	Product selectivity / %							
			Alcohols C_1-C_3		Alcohols C_{4+}	Ketones	Esters	Ethers	Aldehydes	
			C–C cleavage[a]	C–O cleavage[b]						
Ir/SiO_2	21.2	0.05	2.9	71.8	1.5	8.1	7.2	7.9	0.4	
Ir/γ-Al_2O_3	57.2	0.16	3.8	42.3	10.0	18.9	7.4	11.7	1.0	
Ir/ZrO_2	65.3	0.22	1.6	34.5	12.4	19.7	15.5	10.5	0.9	

[a]C–C cleavage alcohols: methanol, ethanol, ethylene glycol; [b]C–O cleavage alcohols:propanol, 1,2-propanediol, 1,3-propanediol. TOF: turnover frequency.

reaction, since the pressure increase had an insignificant effect on conversion and selectivity over Ir/SiO_2.

In summary, the main products for the three catalysts were short chain alcohols (C_1-C_3), the typical glycerol hydrogenolysis products, including methanol, ethanol, propanol, ethylene glycol, 1,2-PDO and 1,3-PDO. Ir/SiO_2 showed the highest selectivity to C_1-C_3 alcohols (74.7%), whereas the Ir/γ-Al_2O_3 and Ir/ZrO_2 catalysts had selectivity for short chain alcohols of 46.1 and 36.1%, respectively. For all catalysts, 1-propanol was the main product, with selectivities of 46.7% for Ir/SiO_2, 30.9% for Ir/γ-Al_2O_3 and 29.6% when using Ir/ZrO_2. Besides, 1,2-PDO was the product with the second highest selectivity among the alcohols: 24.4% for Ir/SiO_2, 8.5% for Ir/γ-Al_2O_3 and 2.8% for Ir/ZrO_2. Furthermore, 1,3-PDO was also formed with a selectivity of 0.6% for Ir/SiO_2, 2.7% for Ir/γ-Al_2O_3 and 1.8% for Ir/ZrO_2. These results can be attributed to the elevated temperature of the reaction, which could have led 1,2-PDO and 1,3-PDO to further react and form 1-propanol by dehydration, according to reaction mechanisms studies starting from the main products of glycerol hydrogenolysis.[43,44]

In these reaction conditions, C–O cleavage was favored, and the trend for C–C cleavage in the selectivity of short chain alcohols was Ir/γ-Al_2O_3 > Ir/SiO_2 > Ir/ZrO_2 (Table 5). Ir/γ-Al_2O_3 and Ir/SiO_2 catalysts presented similar selectivities for alcohols produced by C–C cleavage (methanol and ethylene glycol), higher than those obtained for Ir/ZrO_2, as observed for cyclohexane hydrogenolysis, where Ir/ZrO_2 presented the lowest selectivity for products formed by subsequent hexane hydrogenolysis. Thus, these results can indicate that both C–O and C–C hydrogenolysis are influenced by acidic properties of the support, the electronic state of the active phase and the different metal-support interactions.[48]

The distribution of oxygenated products formed in the reactions with Ir/γ-Al_2O_3 and Ir/ZrO_2 was interesting. Ir/ZrO_2 presented a selectivity to esters of 15.5%, whereas Ir/γ-Al_2O_3 displayed a selectivity of 7.4%. This fact can indicate that Ir/ZrO_2 favored the oxidation of hydrogenolysis products, like alcohols and ketones, by the water present in the reaction media to form more oxygenated products including esters and carboxylic acids.[49]

Conclusions

Cyclohexane conversion and glycerol hydrogenolysis were used to compare the behavior of iridium catalysts in terms of C–C and C–O cleavage. For cyclohexane hydrogenolysis, Ir/SiO_2 showed the best activity and high selectivities for minor hydrocarbons formed by subsequent hexane hydrogenolysis. On the other hand, Ir/ZrO_2 catalyst showed the lowest activity for cyclohexane hydrogenolysis and the lowest selectivities for minor hydrocarbons. These differences could be attributed to surface characteristics like particle size, adlineaton sites and electronic state of Ir on the supports, which affect directly the re-adsorption of hexane to form minor hydrocarbons. For glycerol hydrogenolysis, the activity increased in the sequence Ir/SiO_2 < Ir/γ-Al_2O_3 < Ir/ZrO_2 in all reaction conditions, the same trend observed for the number of surface active sites

estimated by cyclohexane dehydrogenation model reaction. The effect of the nature of support was more evident on the product selectivity. Although all catalysts favored C–O cleavage, forming products like 1,2-PDO and propanol, Ir/γ-Al$_2$O$_3$ presented the higher selectivity to minor alcohols formed by C–C cleavage such as methanol and ethylene glycol. Ir/ZrO$_2$ catalyst showed the highest activity in all reaction conditions and the lowest selectivity to minor alcohols produced from C–C cleavage. The differences in the state of surface iridium and support properties were responsible for the catalytic behaviors.

Supplementary Information

Supplementary information (liquid products formed in high temperature reactions) is available free of charge at http://jbcs.sbq.org.br as PDF file.

Acknowledgments

References

1. Garin, F.; Girard, P.; Weisang, F.; Maire, G.; *J. Catal.* **1981**, *70*, 215.

2. Din, P. M.; Howarth, J. A.; Hudnott, A. R.; Williams, J. M. J.; *Tetrahedron Lett.* **1996**, *37*, 7623.

3. Cunha, D. S.; Cruz, G. M.; *Appl. Catal., A* **2002**, *236*, 55.

4. Marzialetti, T.; Oportus, M.; Ruiz, D.; Fierro, J. L. G.; Reyes, P.; *Catal. Today* **2008**, *133-135*, 711.

5. Cadu, A.; Andersson, P. G.; *Dalton Trans.* **2013**, *42*, 14345.

6. Xu, Z.; McNamara, N. D.; Neumann, G. T.; Schneider, W. F.; Hicks, J. C.; *ChemCatChem* **2013**, *5*, 1769.

7. Foger, K.; Anderson, J. R.; *J. Catal.* **1979**, *59*, 325.

8. Foger, K.; Anderson, J. R.; *J. Catal.* **1980**, *64*, 448.

9. Foger, K.; *J. Catal.* **1982**, *78*, 406.

10. van Senden, J. G.; van Broekhoven, E. H.; Wreesman, C. T. J.; Ponec, V.; *J. Catal.* **1984**, *87*, 468.

11. Walter, C. G.; Coq, B.; Figueras, F.; Boulet, M.; *Appl. Catal., A* **1995**, *133*, 95.

12. McVicker, G.; Daage, M.; Touvelle, M. S.; Hudson, C. W.; Klein, D. P.; Baird Jr., W. C.; Cook, B. R.; Chen, J. G.; Hantzer, S.; Vaughan, D. E. W.; Ellis, E. S.; Feeley, O. C.; *J. Catal.* **2002**, *210*, 137.

13. Rodríguez-Gattorno, G.; Alemán-Vázquez, L. O.; Angeles-Franco, X.; Cano-Domínguez, J. L.; Villagómez-Ibarra, R.; *Energy Fuels* **2007**, *21*, 1122.

14. Shi, H.; Li, X.; Haller, G. L.; Gutiérrez, O. Y.; Lercher, J. A.; *J. Catal.* **2012**, *295*, 133.

15. Passos, F.; Fréty, R.; Schmal, M.; *Catal. Lett.* **1994**, *29*, 109.

16. Aranda, D. A. G.; Ramos, A. D.; Passos, F. B.; Schmal, M.; *Catal. Today* **1996**, *28*, 119.

17. Passos, F. B.; Aranda, D. A. G.; Schmal, M.; *J. Catal.* **1998**, *178*, 478.

18. Lisboa, J. S.; Santos, D. C. R. M.; Passos, F. B.; Noronha, F. B.; *Catal. Today* **2005**, *101*, 15.

19. Lisboa, J. S.; Maia, M. P.; Moreira, A. P. E.; Passos, F. B. In *Studies in Surface Science and Catalysis*, vol. 167; Noronha, F. B.; Schmal, M.; Sousa-Aguiar, E. F., eds.; Elsevier: Amsterdam, 2007, pp. 165.

20. Lisboa, J. S.; Terra, L. E.; Silva, P. R. J.; Saitovitch, H.; Passos, F. B.; *Fuel Process. Technol.* **2011**, *92*, 2075.

21. Locatelli, F.; Candy, J.-P.; Didillon, B.; Niccolai, G. P.; Uzio, D.; Basset, J.-M.; *J. Am. Chem. Soc.* **2001**, *123*, 1658.

22. Nakagawa, Y.; Shinmi, Y.; Koso, S.; Tomishige, K.; *J. Catal.* **2010**, *272*, 191.

23. Amada, Y.; Shinmi, Y.; Koso, S.; Kubota, T.; Nakagawa, Y.; Tomishige, K.; *Appl. Catal., B* **2011**, *105*, 117.

24. Nakagawa, Y.; Ning, X.; Amada, Y.; Tomishige, K.; *Appl. Catal., A* **2012**, *433-434*, 128.

25. Chen, K.; Mori, K.; Watanabe, H.; Nakagawa, Y.; Tomishige, K.; *J. Catal.* **2012**, *294*, 171.

26. Amada, Y.; Watanabe, H.; Tamura, M.; Nakagawa, Y.; Okumura, K.; Tomishige, K.; *J. Phys. Chem. C* **2012**, *116*, 23503.

27. Zhou, C. H.; Beltramini, J. N.; Fan, Y. X.; Lu, G. Q.; *Chem. Soc. Rev.* **2008**, *37*, 527.

28. Siang, J. Y.; Lee, C. C.; Wang, C. H.; Wang, W. T.; Deng, C. Y.; Yeh, C. T.; Wang, C. B.; *Int. J. Hydrogen Energy* **2010**, *35*, 3456.

29. Tian, H.; Zhang, T.; Sun, X.; Liang, D.; Lin, L.; *Appl. Catal., A* **2001**, *210*, 55.

30. Peuckert, M.; *Surf. Sci.* **1984**, *144*, 451.

31. Atanasoska, L.; Atanasoski, R.; Trasatti, S.; *Vacuum* **1990**, *40*, 91.

32. Riga, J.; Tenret-Noël, C.; Pireaux, J. J.; Caudano, R.; Verbist, J. J.; Gobillon, Y.; *Phys. Scr.* **1977**, *16*, 351.

33. Folkesson, B.; *Acta Chem. Scand.* **1973**, *27*, 287.

34. Kim, Y. I.; Hatfield, W. E.; *Inorg. Chim. Acta* **1991**, *188*, 15.

35. Bhatia, S.; Beltramini, J.; Do, D. D.; *Catal. Today* **1990**, *7*, 309.

36. Patel, S.; Pant, K. K.; *Fuel Process. Technol.* **2007**, *88*, 825.

37. Velu, S.; Kapoor, M. P.; Inagaki, S.; Suzuki, K.; *Appl. Catal., A* **2003**, *245*, 317.

38. Krishnamurthy, S.; Landolt, G. R.; Schoennagel, H. J.; *J. Catal.* **1982**, *78*, 319.

39. Souza, M. M. V. M.; Schmal, M.; *Appl. Catal., A* **2005**, *281*, 19.

40. Shi, H.; Gutiérrez, O. Y.; Haller, G. L.; Mei, D.; Rousseau, R.; Lercher, J. A.; *J. Catal.* **2013**, *297*, 70.

41. Sinfelt, J. H.; *Catal. Rev.* **1970**, *3*, 175.

42. Salazar, J. B.; Falcone, D. D.; Pham, H. N.; Datye, A. K.; Passos, F. B.; Davis, R. J.; *Appl. Catal., A* **2014**, *482*, 137.

43. Kusunoki, Y.; Miyazawa, T.; Kunimori, K.; Tomishige, K.; *Catal. Commun.* **2005**, *6*, 645.

44. Miyazawa, T.; Koso, S.; Kunimori, K.; Tomishige, K.; *Appl. Catal., A* **2007**, *329*, 30.

45. Delgado, S. N.; Yap, D.; Vivier, L.; Especel, C.; *J. Mol. Catal. A: Chem.* **2013**, *367*, 89.

46. Hong, X.; Lu, J.-q.; Li, B.; Jin, L.-y.; Hu, G.-s.; Wang, Y.-j.; Luo, M.-f.; *Indian J. Chem., Sect. A: Inorg., Bio-inorg., Phys., Theor. Anal. Chem.* **2013**, *52*, 28.

47. Reyes, P.; Aguirre, M. C.; Pecchi, G.; Fierro, J. L. G.; *J. Mol. Catal. A: Chem.* **2000**, *164*, 245.

48. Chen, L.; Zhu, Y.; Zheng, H.; Zhang, C.; Zhang, B.; Li, Y.; *J. Mol. Catal. A: Chem.* **2011**, *351*, 217.

49. Florez-Rodriguez, P. P.; Pamphile-Adrián, A. J.; Passos, F. B.; *Catal. Today* **2014**, *237*, 38.